Self-Generated Plasma Rotation in a Z-Pinch Implosion with Preembedded Axial Magnetic Field

M. Cvejić,[1,*] D. Mikitchuk,[1,2] E. Kroupp,[1] R. Doron,[1] P. Sharma,[1] Y. Maron,[1] A. L. Velikovich,[3] A. Fruchtman,[4] I. E. Ochs,[5] E. J. Kolmes,[5] and N. J. Fisch[5]

[1]*Weizmann Institute of Science, Rehovot 7610001, Israel*
[2]*Ecole polytechnique fèdèrale de Lausanne (EPFL), Route Cantonale, 1015 Lausanne, Switzerland*
[3]*Plasma Physics Division, Naval Research Laboratory, Washington, D.C. 20375, USA*
[4]*Holon Institute of Technology, P.O. Box 305, Holon 58102, Israel*
[5]*Department of Astrophysical Sciences, Princeton University, Princeton, New Jersey 08540, USA*

(Received 13 April 2021; revised 25 October 2021; accepted 15 December 2021; published 5 January 2022)

Using detailed spectroscopic measurements, highly resolved in both time and space, a self-generated plasma rotation is demonstrated using a cylindrical implosion with a preembedded axial magnetic field (B_{z0}). The rotation direction is found to depend on the direction of B_{z0} and its velocity is found comparable to the peak implosion velocity, considerably affecting the force and energy balance throughout the implosion. Moreover, the evolution of the rotation is consistent with magnetic flux surface isorotation, a novel observation in a Z pinch, which is a prototypical time dependent system.

DOI: 10.1103/PhysRevLett.128.015001

Z-pinch implosions with preembedded axial magnetic fields (B_{z0}) have been intensely studied during the last decade [1–18] due to their importance both for inertial confinement fusion [1,2,8,9] and for the study of fundamental plasma physics [19,20]. To induce rotation in Z pinches, precursor plasma jets have been rotated by twisting a wire array [21] or using a radial cusp field [22]. Here, we show for the first time that rotation can be naturally induced by embedding an axial magnetic field. Embedding an axial field means that during the implosion not only is the plasma compressed but also the axial magnetic field. Naturally, the implosion dynamics is then affected by the thermal and compressed B_z counterpressure. However, as we now observe, the plasma also rotates spontaneously, with the rotation velocity comparable to the implosion velocity. We show that such a rotation affects significantly the implosion dynamics through the centrifugal force and instability mitigation. This result can be highly important for magnetized-plasma compression in general and in particular for the Magnetized Liner Inertial Fusion approach to inertial confinement fusion [1–4,8,9].

Remarkably, the evolution of rotation velocity is found to be consistent with isorotation. According to a classic result of axisymmetric magnetohydrodynamics, in steady state, the plasma along each magnetic flux surface should rotate at the same angular frequency. This so-called "isorotation" is important in many steady-state laboratory devices such as Hall thrusters [23–27], centrifugal mirror fusion [28,29], plasma mass filters [30,31], and in some models of accretion disk collapse [32–35]. Here, we demonstrate, that in a Z-pinch implosion with an embedded axial field, a distinctly non-steady-state system, the rotation profiles observed are consistent with a tendency toward isorotation, with the arrival toward isorotation occurring on the same timescale as the implosion.

The phenomena discovered here are investigated by unique spectroscopic measurements of azimuthal and axial B field, the ion radial and azimuthal velocities, and the plasma parameters, employed simultaneously thus enabling the examination of both the B-field distribution and rotation profile throughout the implosion. This information allows for a quantitative study of the rotation parameters and the energy balance, informing on the mechanism of the rotation. The consistency with isorotation suggests a valuable laboratory platform to explore plasma rotation in a variety of systems, including space [36] and plasma devices, e.g., [37–40].

Figure 1(a) shows a schematic of the experimental and diagnostic setups. A cylindrical oxygen-puff shell with initial outer and inner radii of 19 and 7 mm, respectively, and mass $\sim 10\ \mu g/cm$, as determined by interferometry, prefills the A-K gap with a preembedded, quasistatic axial magnetic flux ($B_{z0} = 0.26$ T). B_{z0} is generated by a pair of Helmholtz coils, rising in ~ 95 ms, to allow for the diffusion of B_{z0} into the vacuum chamber and the A-K gap. Subsequently, a pulsed current (rising to 300 kA in 1.6 μs) is driven through the gas, ionizes it, and generates an azimuthal magnetic field that compresses the plasma radially inward together with the embedded B_z field. The time of the peak plasma compression (denoted in this paper as $t = 0$), determined by the peak of a ultraviolet-to-visible photodiode signal that coincides with the minimum plasma radius seen in 2D images, occurs, for $B_{z0} = 0.26$ T, ~ 700 ns after the current initiation. An absolutely calibrated B-dot probe measures the total current.

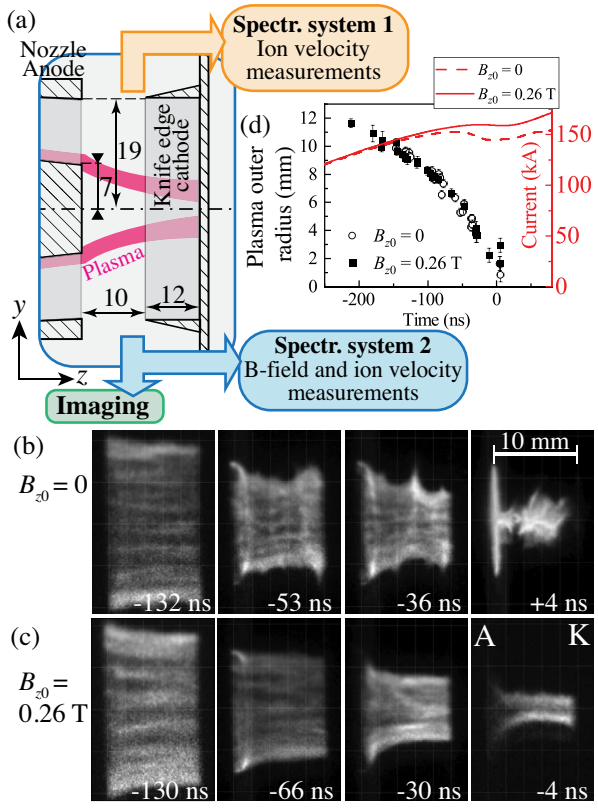

FIG. 1. (a) Schematic description of the experimental setup and spectroscopic systems showing the geometry of the electrodes in mm in the vicinity of the A-K gap. The Helmholtz coils for the B_{z0} generation (not shown) are outside the vacuum chamber. Spectroscopic system 1: the spectral resolution is 0.7 Å and spatial resolution is < 0.2 mm. Spectroscopic system 2: the spectral resolution is 0.3 Å and spatial resolution is ≈ 0.7 mm. (b) The 5-ns gated 2D plasma images for $B_{z0} = 0$. (c) The 2D plasma images for $B_{z0} = 0.26$ T. (d) Plasma radius, hollow circles and black squares, and current evolution, dashed and solid line, for $B_{z0} = 0$ and for $B_{z0} = 0.26$ T, respectively.

The diagnostic setup allows for recording spatially and temporally resolved data, simultaneously obtaining the parameters of the plasma, B fields, and ion motion. It consists of two imaging ultraviolet-to-visible spectroscopic systems and a 2D imaging system. Details of the diagnostic system shown in Fig. 1(a) are given in [15,20,41,42]. The lines of sight of both systems are perpendicular to the pinch axis. The radial distribution of the ion velocities, B field, and plasma parameters are obtained by taking advantage of the radial separation of the ion charge states during the implosion, that allowed for local measurements in r [20,41,43,44]. Transitions of four charge states (O III $\lambda =$ 3791 Å, O IV $\lambda = 2806$ Å, O V $\lambda = 2781$ Å, and O VI $\lambda = 3811$ Å) were recorded simultaneously for the determination of the v_θ radial distribution.

Figures 1(b) and (c) show 2D images of the plasma self-emission for $B_{z0} = 0$ [Fig. 1(b)] and for $B_{z0} =$ 0.26 T [Fig. 1(c)]. The mitigation of instabilities seen for $B_{z0} = 0.26$ T is consistent with [7]. These images are used for the determination of the outer plasma radius evolution. The outer plasma radius is defined as the radial position of half-peak intensity after inverse Abel transform of the image. The evolution of the outer plasma radius at $z =$ 5 mm and the current traces are shown in Fig. 1(d) for $B_{z0} = 0$ and for $B_{z0} = 0.26$ T. The current drop at stagnation is due to the rise of the plasma impedance. The current traces with $B_{z0} = -0.26/+0.26$ T are indistinguishable.

Figure 2 illustrates the influence of B_z on the plasma rotation. The 2D images in Figs. 2(a)–(c) (left column) show the plasma shape at stagnation for $B_{z0} = 0, +0.26$ T, and -0.26 T, respectively. The white rectangle in each image shows the region where the radially resolved spectra of the O VI 3811.35 Å line, presented in the middle column, are taken from. The white dashed horizontal lines mark the radial extent of the space at the opposite azimuths from which the lineouts are taken, i.e., at $y = \pm r^{\mathrm{O\,VI}}$, where $r^{\mathrm{O\,VI}}$ is the outermost radius of the O VI emission, defined as the r position of half-peak emission as it drops toward the larger radius. The respective line shapes and their best fits are presented in the right column. We determine the rotation velocities from the Doppler-shifted line emission in the opposite azimuths (at $+r$ and $-r$). The rotation velocity

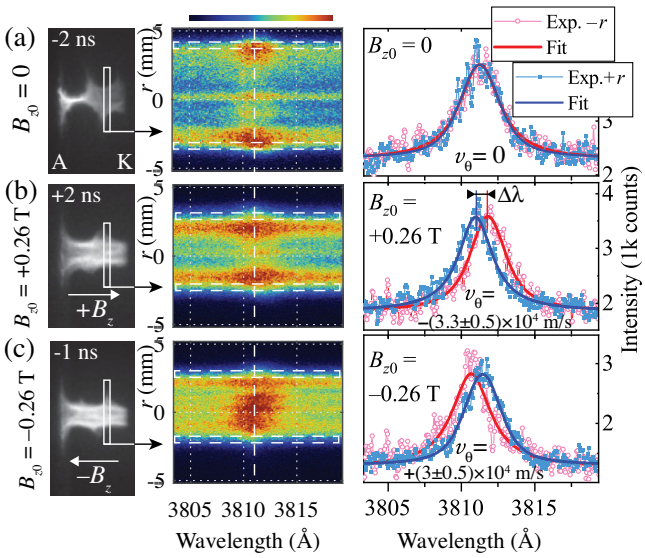

FIG. 2. The left column shows 2D images of the plasma self-emission (in visible). The middle column shows the spectral images of the chordally integrated O VI 3811.35 Å transition (marked by the vertical dashed line) recorded at $z = 7$ mm (the position that is marked by the white rectangle on the 2D images). The right column shows the line shapes of the O VI transition together with the best fits. They are obtained from the lineouts of the spectral images taken at the y positions marked by the dashed white rectangles. The Doppler shifts due to rotation are symmetric around the unshifted wavelength. (a) For $B_{z0} = 0$, $t = -2$ ns; (b) for $B_{z0} = +0.26$ T, $t = 2$ ns; (c) for $B_{z0} = -0.26$ T, $t = -1$ ns.

is given by $v_\theta = \frac{1}{2}c(\Delta\lambda/\lambda_0)$, where c is the speed of light, λ_0 is the transition wavelength, and $\Delta\lambda$ is the difference between the Doppler-shifted line centers for $+r$ and $-r$ [Figs. 2(a)–(c)]. Additional details of the rotation-velocity measurement are given in the Supplemental Material [45]. In Fig. 2(a), for $B_{z0} = 0$, no Doppler shift between the line shapes at opposite azimuths is detected, yielding $v_\theta = 0$. For $B_{z0} = +0.26$ T [B_z directed from anode to cathode, Fig. 2(b)] and for $B_{z0} = -0.26$ T [B_z directed from cathode to anode, Fig. 2(c)] v_θ measured are $-3.3 \pm 0.5 \times 10^4$ m/s and $+3 \pm 0.5 \times 10^4$ m/s, respectively. In both cases, the direction of the angular velocity $\vec{\omega}$ ($\omega = v_\theta/r$) is opposite to the direction of the B_{z0}. Thus, Fig. 2 demonstrates that the plasma rotates only in implosions with $|B_{z0}| > 0$ and that the direction of B_{z0} affects the direction of the plasma rotation.

The particle radial velocity v_r is determined using the line shapes obtained from the $y = 0$ chords, giving the opposite Doppler shifts at the opposite sides of the chord [45]. Additionally, the electron density n_e is determined from the Stark broadening of the fitted spectral lines [46], accounting for the small contributions of the Doppler and instrumental broadenings. The electron temperature T_e is obtained using the intensity ratios of O V and O IV transitions with the aid of a collisional-radiative model [47]. The evolution of the plasma parameters will be discussed in a separate study.

We emphasize that very similar results were obtained in simultaneous measurements from orthogonal directions, showing that our conclusions are unaffected by deviations from axisymmetry.

The plasma velocity measurements are summarized in Fig. 3, giving the radial distribution of v_θ and v_r for different times and z positions. The solid lines in Fig. 3 represent the normalized radial distribution of the square root of the continuum emission averaged over 5522 ± 4 Å. For the relevant T_e range (7–13 eV), it is nearly proportional to the electron density [48]. We emphasize that data for each time (v_θ radial distribution, v_r, and the radial distribution of continuum intensity, represented by the same color) are obtained in a single shot. The typical minimum detectable value for v_θ, determined by the spectral dispersion and signal-to-noise ratio, is $\approx 0.5 \times 10^4$ m/s.

Comparing the v_θ and v_r values presented in Fig. 3 shows that the ratio between the rotation ($E_{\rm rot}$) and implosion ($E_{\rm impl}$) kinetic energies varies significantly in time and in the r and z position, e.g., at $z = 1$ and $t \leq -37$ ns $E_{\rm rot} < 0.1 \times E_{\rm impl}$, while at $z = 9$ and $t = -134$ ns $E_{\rm rot} \geq E_{\rm impl}$.

To understand the significance of the centrifugal force for the implosion dynamics, we estimate the different terms of the equation of motion (radial component):

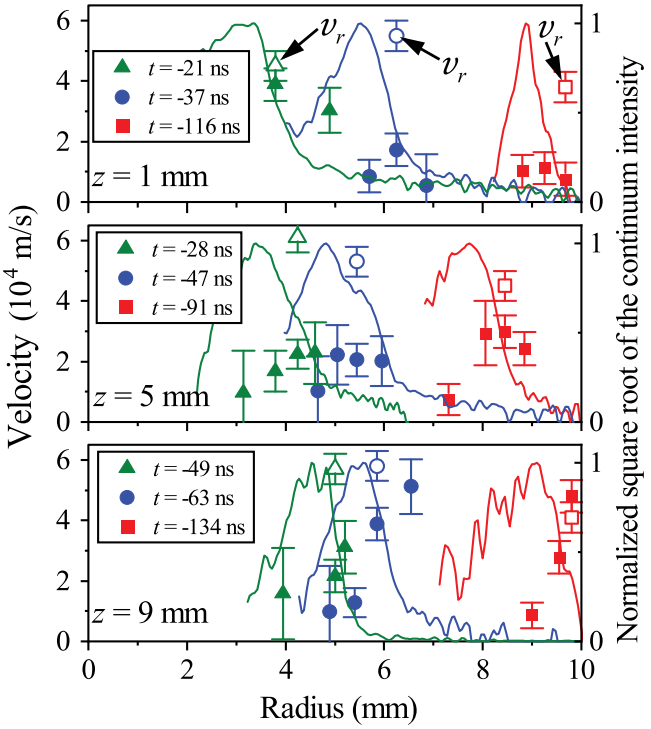

FIG. 3. Radial distribution of v_θ for different times and z positions ($z = 0$ is the anode surface). The corresponding open symbols are the v_r values measured at the radial position of O V. The red, blue, and green lines represent the radial distribution of the square root of the continuum intensity (which is proportional to n_e) at different times and z positions, scaled to unity.

$$\rho\frac{dv_r}{dt} = -\frac{\partial p}{\partial r} - \left(\frac{1}{2\mu_0}\frac{\partial B_\theta^2}{\partial r} + \frac{B_\theta^2}{\mu_0 r}\right) + \frac{1}{2\mu_0}\frac{\partial B_z^2}{\partial r} + \rho\frac{v_\theta^2}{r} = f_T + f_{B_\theta} + f_{B_z} + f_C, \quad (1)$$

where $p = [1 + (1/\bar{Z})]n_e k_B T_e$ is the thermal pressure and ρ is the plasma mass density. For the estimation, we use the measured values at the radial position $r = 9.8$ mm of the O V emission at $z = 9$ mm, and $t = -134$ ns, of $v_\theta = 4.8 \times 10^4$ m/s, $I = 150$ kA, $n_e = 8 \times 10^{23}$ m^{-3}, and $T_e = 9$ eV. $B_\theta = (\mu_0 I/2\pi r)$ is calculated assuming all the current measured by the B-dot probe flows within the plasma outer radius (as confirmed by B_θ measurements). $B_z = B_{z0}(R_0/r)^2$ is calculated assuming ideal B_z flux conservation (also confirmed by B_z measurements). $\Delta r \approx 2$ mm is the length scale of a significant change in the magnitude of B_θ, B_z, and p. It is estimated using the B_θ measurements and the radial distribution of the continuum emission (see Fig. 3). The resultant force density for each term of Eq. (1) is $f_T \approx (p/\Delta r) = 0.7 \pm 0.2 \times 10^9$ N/m^3, $f_{B_\theta} = (1/\mu_0)[\frac{1}{2}(B_\theta^2/\Delta r) + (B_\theta^2/r)] = 3.6 \pm 0.8 \times 10^9$ N/m^3, $f_{B_z} \approx (B_z^2/2\mu_0\Delta r) = 0.2 \pm 0.05 \times 10^9$ N/m^3, and $f_C = \rho(v_\theta^2/r) = 1.5 \pm 0.4 \times 10^9$ N/m^3. It is seen that f_C is the dominant outward acting force, i.e., $f_C > f_{B_z} + f_T$. It is also $\approx 50\%$ of the compressing force f_{B_θ}. Estimates for

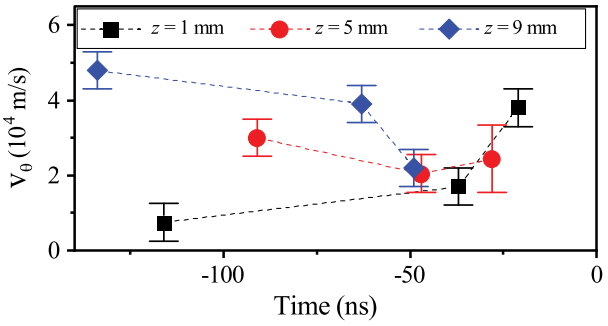

FIG. 4. The evolution of v_θ (with dashed lines as a guide to the eye) as measured at the radial position of O V (see Fig. 3) as a function of time for different axial positions z. Near the cathode ($z = 9$) the rotation slows, while near the anode ($z = 1$) it speeds up.

other times and z positions also show that the centrifugal force plays a significant role in the plasma dynamics during the implosion ($f_C \approx 15\%$–30% of f_{B_θ}).

The rotation might affect the plasma dynamics by mitigating the magneto-Rayleigh-Taylor and magnetohydrodynamics (MHD) instabilities, either by affecting the effective acceleration direction of the Z pinch [49–52] or by phase mixing of an instability perturbation due to the nonuniform angular velocity distribution [53,54]. Indeed, in almost all Z-pinch experiments with preembedded B_z, significant instability mitigation was observed during the implosion and stagnation [3,4,6,7,12,13,16,55,56]. It is a common assumption that the observed stabilization is solely due to the radial bending of the B_z-field lines [57]. However, it is possible that also a self-generated rotation, such as observed here, is partially responsible for the stabilization. For example, adopting the stabilization condition for the kink instability given in [53] due to the sheared plasma velocity, and applying it to our experiment accounting for the nonuniform ω, yields the condition $r(\Delta\omega/\Delta r) > 10^7$ s^{-1} (see the Supplemental Material [45]). From the v_θ distribution at $z = 5$ mm and $t = -28$ ns (Fig. 3), we obtain $r(\Delta\omega/\Delta r) \approx 7 \times 10^6$ s^{-1}, which is close to the condition for stabilization.

Figure 3 shows several trends in the evolution of v_θ. Early in the implosion, the plasma rotates fast near the cathode. The implosion then progresses, with axial asymmetry, as the plasma reaches a smaller radius near the cathode. As demonstrated in Fig. 4, simultaneously, the rotation near the cathode slows down, while the rotation near the anode speeds up, reducing the difference between the rotation speeds at the different parts of the plasma.

This unintuitive evolution of the rotation at different axial positions likely results from the fact that plasma lying on the same magnetic surface tends to rotate at the same frequency [58], as outlined in Ferraro's isorotation theorem [36,59,60] for a steady-state, axisymmetric, magnetized plasma obeying MHD dynamics:

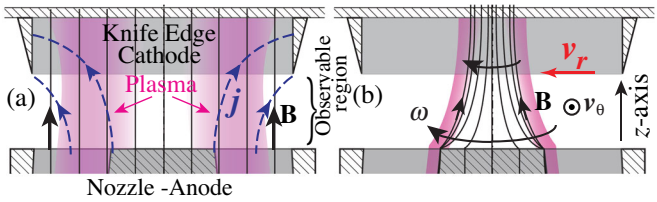

FIG. 5. Schematic of the plasma, electrodes, velocities, and poloidal B field configuration at (a) $t \approx -300$ ns and (b) $t \approx -80$ ns. $\omega = v_\theta/r$ is the rotation angular velocity and $\mathbf{B} = B_z\hat{z} + B_r\hat{r}$ is the magnetic field.

$$\nabla\omega \cdot \mathbf{B} = 0, \tag{2}$$

where ω is the angular rotation frequency and $\mathbf{B}$ is the magnetic field.

Because the magnetic surfaces bend in from large radius at the anode to small radius near the cathode [Fig. 5(b)], isorotation of these surfaces will result in higher rotation velocity near the anode than near the cathode. The trends shown in Fig. 4 are thus consistent with the tendency toward isorotation. As we show in the Supplemental Material [45], the early time gradient of the axial rotation twists the magnetic field lines, creating a torque that tends to push the plasma toward isorotation. This mechanism is sufficient to approach isorotation when the axial magnetic field is large enough for a shear Alfvén wave to propagate across the anode-cathode gap over the implosion time.

The initial rotation of the plasma cannot be understood only based on MHD, since it depends on the initial current breakdown that is determined by the electrode geometry and initial gas distribution. While the anode is a flat surface over large and small radius, the "knife edge" round cathode is located at large radius. Thus, we expect the current to develop a radial component near the cathode, which increases close to the cathode [Fig. 5(a)]. This radial current combines with the B_z to produce a $\mathbf{j} \times \mathbf{B}$ force in the v_θ direction (note that by our convention, the coordinate system (r, z, θ) is right-handed). The torque due to the $\mathbf{j} \times \mathbf{B}$ force initiates rotation near the cathode and causes a faster rotation at radii with lower plasma density (thus with lower inertia) at the outer edge of the plasma, as observed (see Fig. 3 for $z = 9$ mm).

In summary, novel spectroscopic measurements in an imploding Z pinch with an embedded axial magnetic field demonstrated self-generated plasma rotation in Z pinches, with two unusual features, observed here for the first time: (i) the rotation velocity is comparable to the implosion velocity; and (ii) the plasma rotation velocity profile is strikingly consistent with isorotation of the magnetic surfaces, a particularly remarkable feature in an imploding system.

The fact that the rotation velocities are comparable to the implosion velocities means that the associated centrifugal forces have a significant influence on the force and energy

balance. Moreover, the large shear in the rotation suggests that it might exert a stabilizing effect on plasma instabilities, an effect consistent with observations in other rotating plasma experiments, e.g., [39,51]. These observations are of particular importance for the understanding of the implosion dynamics in magnetized Z-pinch configurations designed for fusion purposes or for radiation sources [19].

Moreover, the fact that the rotation is consistent with isorotation now stimulates measurements, in greater detail than provided here, to identify the precise extent of any deviations from isorotation. The magnetized Z pinch, since it is a time-varying plasma that should exhibit deviations, is now identified as a perfect system for studying these deviations. This would then have far reaching applicability in understanding naturally occurring rotating plasma phenomena that are ubiquitous, for example, in astrophysical systems, but hard to diagnose. In particular, the observed rotation transport and magnetic geometry bear marked similarity to the magnetocentrifugal wind model of stellar accretion disk collapse [32–35], where isorotation leads to angular momentum transport outward along the flux surfaces, allowing the disk to collapse and the star to form. While the connection to accretion disk physics is speculative at this stage, it does suggest that study of rotation in laboratory Z pinches might shed light on rotating systems for which the set of detailed measurements as performed here would be impossible.

We thank A. Fisher and U. Shumlak for invaluable suggestions and fruitful discussions and P. Meiri for his skillful assistance. This work was supported in part by the Cornell Multi-University Center for High Energy Density Science (USA) 83228-10969, by Lawrence Livermore National Laboratory B647552, by the USA-Israel Binational Science Foundation 2020292, by NSF-BSF (USA-Israel) 2017669, by NNSA 83228-10966 [Prime No. DOE (NNSA) DE-NA0003764] and by NSF PHY-1805316.

M. C. and D. M. contributed equally to this work.

*Corresponding author.
marko.cvejic@weizmann.ac.il

[1] S. A. Slutz, M. C. Herrmann, R. A. Vesey, A. B. Sefkow, D. B. Sinars, D. C. Rovang, K. J. Peterson, and M. E. Cuneo, Pulsed-power-driven cylindrical liner implosions of laser preheated fuel magnetized with an axial field, Phys. Plasmas **17**, 056303 (2010).

[2] S. A. Slutz and R. A. Vesey, High-Gain Magnetized Inertial Fusion, Phys. Rev. Lett. **108**, 025003 (2012).

[3] T. J. Awe *et al.*, Observations of Modified Three-Dimensional Instability Structure for Imploding *z*-Pinch Liners that are Premagnetized with an Axial Field, Phys. Rev. Lett. **111**, 235005 (2013).

[4] T. J. Awe *et al.*, Modified helix-like instability structure on imploding z-pinch liners that are pre-imposed with a uniform axial magnetic field, Phys. Plasmas **21**, 056303 (2014).

[5] S. A. Sorokin, Gas-puff liner implosion in the configuration with helical current return rods, Plasma Phys. Rep. **39**, 139 (2013).

[6] N. Qi, P. de Grouchy, P. C. Schrafel, L. Atoyan, W. M. Potter, A. D. Cahill, P.-A. Gourdain, J. B. Greenly, D. A. Hammer, C. L. Hoyt, B. R. Kusse, S. A. Pikuz, and T. A. Shelkovenko, Gas puff Z-pinch implosions with external Bz field on COBRA, AIP Conf. Proc. **1639**, 51 (2014).

[7] D. Mikitchuk, C. Stollberg, R. Doron, E. Kroupp, Y. Maron, H. R. Strauss, A. L. Velikovich, and J. L. Giuliani, Mitigation of instabilities in a Z-pinch plasma by a preembedded axial magnetic field, IEEE Trans. Plasma Sci. **42**, 2524 (2014).

[8] M. R. Gomez *et al.*, Experimental Demonstration of Fusion-Relevant Conditions in Magnetized Liner Inertial Fusion, Phys. Rev. Lett. **113**, 155003 (2014).

[9] P. F. Knapp *et al.*, Effects of magnetization on fusion product trapping and secondary neutron spectra, Phys. Plasmas **22**, 056312 (2015).

[10] L. Atoyan, D. A. Hammer, B. R. Kusse, T. Byvank, A. D. Cahill, J. B. Greenly, S. A. Pikuz, and T. A. Shelkovenko, Helical plasma striations in liners in the presence of an external axial magnetic field, Phys. Plasmas **23**, 022708 (2016).

[11] D. A. Yager-Elorriaga, P. Zhang, A. M. Steiner, N. M. Jordan, P. C. Campbell, Y. Y. Lau, and R. M. Gilgenbach, Discrete helical modes in imploding and exploding cylindrical, magnetized liners, Phys. Plasmas **23**, 124502 (2016).

[12] A. G. Rousskikh, A. S. Zhigalin, V. I. Oreshkin, V. Frolova, A. L. Velikovich, G. Y. Yushkov, and R. B. Baksht, Effect of the axial magnetic field on a metallic gas-puff pinch implosion, Phys. Plasmas **23**, 063502 (2016).

[13] A. G. Rousskikh, A. S. Zhigalin, V. I. Oreshkin, and R. B. Baksht, Measuring the compression velocity of a Z pinch in an axial magnetic field, Phys. Plasmas **24**, 063519 (2017).

[14] D. A. Yager-Elorriaga, Y. Y. Lau, P. Zhang, P. C. Campbell, A. M. Steiner, N. M. Jordan, R. D. McBride, and R. M. Gilgenbach, Evolution of sausage and helical modes in magnetized thin-foil cylindrical liners driven by a Z-pinch, Phys. Plasmas **25**, 056307 (2018).

[15] D. Mikitchuk, M. Cvejić, R. Doron, E. Kroupp, C. Stollberg, Y. Maron, A. L. Velikovich, N. D. Ouart, J. L. Giuliani, T. A. Mehlhorn, E. P. Yu, and A. Fruchtman, Effects of a Preembedded Axial Magnetic Field on the Current Distribution in a *Z*-Pinch Implosion, Phys. Rev. Lett. **122**, 045001 (2019).

[16] F. Conti, N. Aybar, J. Narkis, J. C. Valenzuela, H. U. Rahman, E. Ruskov, E. Dutra, S. Haque, A. Covington, and F. N. Beg, Study of stability in a liner-on-target gas puff Z-pinch as a function of pre-embedded axial magnetic field, Phys. Plasmas **27**, 012702 (2020),

[17] P. C. Campbell, T. M. Jones, J. M. Woolstrum, N. M. Jordan, P. F. Schmit, J. B. Greenly, W. M. Potter, E. S. Lavine, B. R. Kusse, D. A. Hammer, and R. D. McBride, Stabilization of Liner Implosions via a Dynamic Screw Pinch, Phys. Rev. Lett. **125**, 035001 (2020).

[18] C. E. Seyler, Axial magnetic flux amplification in Hall-magnetohydrodynamic simulations of externally magnetized z-pinches, Phys. Plasmas **27**, 092102 (2020).
[19] J. L. Giuliani and R. J. Commisso, A review of the gas-puff *Z*-pinch as an x-ray and neutron source, IEEE Trans. Plasma Sci. **43**, 2385 (2015).
[20] Y. Maron, Experimental determination of the thermal, turbulent, and rotational ion motion and magnetic field profiles in imploding plasmas, Phys. Plasmas **27**, 060901 (2020).
[21] D. J. Ampleford, S. V. Lebedev, A. Ciardi, S. N. Bland, S. C. Bott, G. N. Hall, N. Naz, C. A. Jennings, M. Sherlock, J. P. Chittenden, J. B. A. Palmer, A. Frank, and E. Blackman, Supersonic Radiatively Cooled Rotating Flows and Jets in the Laboratory, Phys. Rev. Lett. **100**, 035001 (2008).
[22] M. J. Bennett, S. V. Lebedev, G. N. Hall, L. Suttle, G. Burdiak, F. Suzuki-Vidal, J. Hare, G. Swadling, S. Patankar, M. Bocchi, J. P. Chittenden, R. Smith, A. Frank, E. Blackman, R. P. Drake, and A. Ciardi, Formation of radiatively cooled, supersonically rotating, plasma flows in Z-pinch experiments: Towards the development of an experimental platform to study accretion disk physics in the laboratory, High Energy Density Phys. **17**, 63 (2015).
[23] A. Smirnov, Y. Raitses, and N. J. Fisch, Experimental and theoretical studies of cylindrical Hall thrusters, Phys. Plasmas **14**, 057106 (2007).
[24] N. J. Fisch, Y. Raitses, and A. Fruchtman, Ion acceleration in supersonically rotating magnetized-electron plasma, Plasma Phys. Controlled Fusion **53**, 124038 (2011).
[25] Y. Gao, H. Liu, P. Hu, H. Huang, and D. Yu, The effect of magnetic field near the anode on cylindrical Hall thruster, Plasma Sources Sci. Technol. **25**, 035011 (2016).
[26] Y. Jiang, H. Tang, J. Ren, M. Li, and J. Cao, Magnetic mirror effect in a cylindrical Hall thruster, J. Phys. D **51**, 035201 (2018).
[27] S. Liang, H. Liu, and D. Yu, Effect of permanent magnet configuration on discharge characteristics in cylindrical Hall thrusters, Phys. Lett. A **383**, 2272 (2019).
[28] A. A. Bekhtenev, V. I. Volosov, V. E. Pal'Chikov, M. S. Pekker, and Y. N. Yudin, Problems of a thermonuclear reactor with a rotating plasma, Nucl. Fusion **20**, 579 (1980).
[29] V. I. Volosov, Aneutronic fusion on the base of asymmetrical centrifugal trap, Nucl. Fusion **46**, 820 (2006).
[30] A. J. Fetterman and N. J. Fisch, The magnetic centrifugal mass filter, Phys. Plasmas **18**, 094503 (2011).
[31] R. Gueroult, J.-M. Rax, and N. J. Fisch, The double well mass filter, Phys. Plasmas **21**, 020701 (2014).
[32] A. Konigl and R. E. Pudritz, Disk winds and the accretion–outflow connection, arXiv:astro-ph/9903168.
[33] R. Salmeron, A. Königl, and M. Wardle, Wind-driving protostellar accretion discs—II. Numerical method and illustrative solutions, Mon. Not. R. Astron. Soc. **412**, 1162 (2011).
[34] X. N. Bai and J. M. Stone, Wind-driven accretion in protoplanetary disks. I. Suppression of the magnetorotational instability and launching of the magnetocentrifugal wind, Astrophys. J. **769**, 76 (2013).
[35] W. Béthune, G. Lesur, and J. Ferreira, Global simulations of protoplanetary disks with net magnetic flux: I. Non-ideal MHD case, Astron. Astrophys. **600**, A75 (2017).
[36] R. M. Kulsrud, *Plasma Physics for Astrophysics* (Princeton University Press, Princeton, NJ, 2010).
[37] R. Gueroult, S. J. Zweben, N. J. Fisch, and J.-M. Rax, E × B configurations for high-throughput plasma mass separation: An outlook on possibilities and challenges, Phys. Plasmas **26**, 043511 (2019).
[38] S. V. Lebedev, A. Frank, and D. D. Ryutov, Exploring astrophysics-relevant magnetohydrodynamics with pulsed-power laboratory facilities, Rev. Mod. Phys. **91**, 025002 (2019).
[39] T. Byvank, J. T. Banasek, W. M. Potter, J. B. Greenly, C. E. Seyler, and B. R. Kusse, Applied axial magnetic field effects on laboratory plasma jets: Density hollowing, field compression, and azimuthal rotation, Phys. Plasmas **24**, 122701 (2017).
[40] D. D. Ryutov, Using intense lasers to simulate aspects of accretion discs and outflows in astrophysics, Astrophys. Space Sci. **336**, 21 (2011).
[41] G. Rosenzweig, E. Kroupp, A. Fisher, and Y. Maron, Measurements of the spatial magnetic field distribution in a z-pinch plasma throughout the stagnation process, J. Instrum. **12**, P09004 (2017).
[42] D. Mikitchuk, *Investigation of the Compression of Magnetized Plasma and Magnetic Flux*, Springer Theses (Springer International Publishing, New York, 2019), https://link.springer.com/book/10.1007%2F978-3-030-20855-4.
[43] G. Davara, L. Gregorian, E. Kroupp, and Y. Maron, Spectroscopic determination of the magnetic field distribution in an imploding plasma, Phys. Plasmas **5**, 1068 (1998).
[44] G. Rosenzweig, E. Kroupp, T. Queller, A. Starobinets, Y. Maron, V. Tangri, J. L. Giuliani, and A. Fruchtman, Local measurements of the spatial magnetic field distribution in a z-pinch plasma during and near stagnation using polarization spectroscopy, Phys. Plasmas **27**, 022705 (2020).
[45] See Supplemental Material at http://link.aps.org/supplemental/10.1103/PhysRevLett.128.015001 for (i) Principle of simultaneous measurements of plasma rotation and implosion, (ii) Estimation of the stability criterion due to radial shear of angular velocity, (iii) Isorotation in a compressing plasma.
[46] S. Sahal-Bréchot and M. S. Dimitrijević, and N. Moreau (2021), STARK-B database, [online]. http://stark-b.obspm.fr [June 24, 2020]. Observatory of Paris, LERMA and Astronomical Observatory of Belgrade.
[47] Y. V. Ralchenko and Y. Maron, Accelerated recombination due to resonant deexcitation of metastable states, J. Quant. Spectrosc. Radiat. Transfer **71**, 609 (2001).
[48] H. R. Griem, *Plasma Spectroscopy* (McGraw-Hill Book Company, New York, 1964).
[49] N. Rostoker, C. G. Peterson, and H. Tahsiri, Spin control of the Rayleigh-Taylor instability in high-density Z-pinch, in *Proceedings of the 10th International Conference on High Power Particle Beams, (San Diego, CA)* (IEEE, Piscataway, 1994), p. 773, https://searchworks.stanford.edu/view/10249526.
[50] A. L. Velikovich and J. Davis, Implosions, equilibria, and stability of rotating, radiating Z-pinch plasmas, Phys. Plasmas **2**, 4513 (1995).

[51] P. J. Turchi, A. L. Cooper, R. Ford, and D. J. Jenkins, Rotational Stabilization of an Imploding Liquid Cylinder, Phys. Rev. Lett. **36**, 1546 (1976).

[52] J. Huneault, D. Plant, and A. J. Higgins, Rotational stabilisation of the Rayleigh-Taylor instability at the inner surface of an imploding liquid shell, J. Fluid Mech. **873**, 531 (2019).

[53] U. Shumlak and C. W. Hartman, Sheared Flow Stabilization of the $m = 1$ Kink Mode in Z Pinches, Phys. Rev. Lett. **75**, 3285 (1995).

[54] U. Shumlak, R. P. Golingo, B. A. Nelson, and D. J. Den Hartog, Evidence of Stabilization in the Z-Pinch, Phys. Rev. Lett. **87**, 205005 (2001).

[55] F. S. Felber, F. J. Wessel, N. C. Wild, H. U. Rahman, A. Fisher, C. M. Fowler, M. A. Liberman, and A. L. Velikovich, Ultrahigh magnetic fields produced in a gas-puff Z pinch, J. Appl. Phys. **64**, 3831 (1988).

[56] F. S. Felber, M. M. Malley, F. J. Wessel, M. K. Matzen, M. A. Palmer, R. B. Spielman, M. A. Liberman, and A. L. Velikovich, Compression of ultrahigh magnetic fields in a gas-puff Z pinch, Phys. Fluids **31**, 2053 (1988).

[57] A. B. Bud'ko, F. S. Felber, A. I. Kleev, M. A. Liberman, and A. L. Velikovich, Stability analysis of dynamic Z pinches and theta pinches, Phys. Fluids B **1**, 598 (1989).

[58] B. Lehnert, Rotating plasmas, Nucl. Fusion **11**, 485 (1971).

[59] V. C. A. Ferraro, The Non-uniform Rotation of the Sun and its Magnetic Field, Mon. Not. R. Astron. Soc. **97**, 458 (1937).

[60] H. Alfvén and C. G. Fälthammar, *Cosmical Electrodynamics, Fundamental Principals* (Oxford University Press, New York, 1963).